Available online at www.sciencedirect.com
ScienceDirect
Journal of Sound and Vibration 299 (2007) 977–989
JOURNAL OF SOUND AND VIBRATION
www.elsevier.com/locate/jsvi

A chaos detectable and time step-size adaptive numerical scheme for nonlinear dynamical systems

Yung-Wei Chen[a], Chein-Shan Liu[b], Jiang-Ren Chang[a,*]

[a]*Department of Systems Engineering & Naval Architecture, National Taiwan Ocean University, 2, Pei-Ning Road, Keelung 20224, Taiwan, ROC*
[b]*Department of Mechanical and Mechatronic Engineering, National Taiwan Ocean University, 2, Pei-Ning Road, Keelung 20224, Taiwan, ROC*

Received 22 December 2005; received in revised form 31 July 2006; accepted 3 August 2006
Available online 16 October 2006

Abstract

The first step in investigation the dynamics of a continuous time system described by ordinary differential equations is to integrate them to obtain trajectories. In this paper, we convert the group-preserving scheme (GPS) developed by Liu [International Journal of Non-Linear Mechanics 36 (2001) 1047–1068] to a time step-size adaptive scheme, $x_{\ell+1} = x_\ell + h\mathbf{f}(\mathbf{x}_\ell, t_\ell)$, where $\mathbf{x} \in \mathsf{R}^n$ is the system variables we are concerned with, and $\mathbf{f}(\mathbf{x}, t) \in \mathsf{R}^n$ is a time-varying vector field. The scheme has the form similar to the Euler scheme, $\mathbf{x}_{\ell+1} = \mathbf{x}_\ell + \Delta t\mathbf{f}(\mathbf{x}_\ell, t_\ell)$, but our step-size h is adaptive automatically. Very interestingly, the ratio $h/\Delta t$, which we call the adaptive factor, can forecast the appearance of chaos if the considered dynamical system becomes chaotical. The numerical examples of the Duffing equation, the Lorenz equation and the Rossler equation, which may exhibit chaotic behaviors under certain parameters values, are used to demonstrate these phenomena. Two other non-chaotic examples are included to compare the performance of the GPS and the adaptive one.

1. Introduction

There have a lot of examples to show that the standard discretization methods of differential equations often produce difference equations that do not correspond to the dynamics of the original equations. For examples, Chen and Solis [1] investigated the appearance of spurious solutions when some first-order ODEs are discretized by using the Runge–Kutta methods, and showed that the resulting schemes may produce unrelated bifurcation phenomena to the original equations. Undoubtedly, a major difficultly in the numerical solutions is the existence of numerical instabilities. Mickens [2] has attributed these instabilities into the following four mechanisms: (a) for the central difference scheme, the numerical instabilities are a consequence of the order of the difference scheme being higher than the order of the differential equation; (b) for the forward Euler scheme, the numerical instabilities arise when the step-size is larger than some fixed finite value;

*Corresponding author. Tel.: +886 2 24622192x6031; fax: +886 2 24625945.
E-mail address: cjr@mail.ntou.edu.tw (J.-R. Chang).

0022-460X/$ - see front matter © 2006 Published by Elsevier Ltd.
doi:10.1016/j.jsv.2006.08.028

(c) for the implicit backward Euler scheme, the numerical instabilities occur when the step-size is larger than some fixed finite value, such that all the fixed points of the difference scheme become stable; (d) for the higher-order Runge–Kutta scheme, the numerical instabilities occur when the step-size is larger than some fixed finite value, such that some spurious fixed points of the difference scheme appear. As a result, the step-size for the scheme being used is usually controlled by the stability considerations and therefore, is very small. How to develop an effective variable step-size numerical scheme for saving computational time and ensuring accuracy is now a major study area in numerical methods.

In order to deal with those difficulties appeared in the conventional numerical methods, a group-preserving scheme (GPS) that focuses to preserve the group properties of the considered system has been developed by Liu [3] through embedding the general nonlinear dynamical system into an augmented dynamical system. Thus, for the general dynamical system of ordinary differential equations it can be endowed a cone structure on the Minkowski space, of which a proper orthochronous Lorentz group left acts. Mathematically speaking, the general dynamical system with dimension n exhibits an internal symmetry group SO_o $(n, 1)$, and the so-called GPS to preserve the group SO_o $(n, 1)$ in the numerical time stepping can be developed.

A deterministic system is said to be chaotic whenever its evolution sensitively depends on the initial conditions. The necessary requirements for a deterministic system to be chaotic are that the system must be nonlinear and be at least three dimensional [4]. This property implies that two trajectories emerging from two different nearby initial conditions separate exponentially in the course of time. In order to realize a desirable (chaotic, periodic, or stationary) behavior, controls of chaos referring to a process wherein a tiny perturbation is applied to a chaotic system are arising and applying in many fields. An important article addressing the control of chaos including of theory and applications [4] can be found. The fact that some dynamical model systems showing the above necessary conditions possess such a critical dependence on the initial condition has now been known. In fact, chaotic systems are common in nature and recently, remedies and applications to the fields of vibration problems have been emerged [5–9].

In this paper, we will convert the GPS to a time step-size adaptive scheme. This scheme has the form similar to the Euler scheme, but its step-size is adaptive automatically, which can forecast the appearance of chaotical behavior of the considered dynamical system under certain values of the parameters.

2. Group-preserving scheme

The group-preserving scheme is such a scheme that can preserve the internal symmetry group of the considered system. Although we do not know previously what kind symmetry group of the general nonlinear dynamical systems have, yet Liu [3] has embedded them into the augmented dynamical systems, which concern with not only the evolutions of the state variable itself but also with the evolution of its magnitude. That is, for the general dynamical system of n ordinary differential equations:

$$\dot{\mathbf{x}} = \mathbf{f}(\mathbf{x}, t), \quad \mathbf{x} \in \mathsf{R}^n, \quad t \in \mathsf{R}, \tag{1}$$

we can embed it into the following $(n+1)$-dimensional augmented dynamical system:

$$\frac{\mathrm{d}}{\mathrm{d}t}\begin{bmatrix} \mathbf{x} \\ ||\mathbf{x}|| \end{bmatrix} = \begin{bmatrix} 0_{n\times n} & \frac{\mathbf{f}(\mathbf{x},t)}{||\mathbf{x}||} \\ \frac{\mathbf{f}^{\mathrm{T}}(\mathbf{x},t)}{||\mathbf{x}||} & 0 \end{bmatrix} = \begin{bmatrix} \mathbf{x} \\ ||\mathbf{x}|| \end{bmatrix}. \tag{2}$$

Here we assure that $\mathbf{x}$ never goes to the zero point, which leads to $||\mathbf{x}|| > 0$ and hence, the above system is well defined. It is obvious that the first equation in Eq. (2) is the same as the original Eq. (1), but the addition of the second equation gives us a Minkowskian structure with the augmented state variable $\mathbf{X} := (\mathbf{x}^{\mathrm{T}}, ||\mathbf{x}||)^{\mathrm{T}}$ satisfying the cone condition

$$\mathbf{X}^{\mathrm{T}}\mathbf{g}\mathbf{X} = 0, \tag{3}$$

where

$$\mathbf{g} = \begin{bmatrix} \mathbf{I}_n & 0_{n\times 1} \\ 0_{1\times n} & -1 \end{bmatrix} \tag{4}$$

is a Minkowski metric. $\mathbf{I}_n$ is the identity matrix of order n, and the superscript T stands for the transpose. In terms of $(\mathbf{x}, ||\mathbf{x}||)$, Eq. (3) becomes

$$\mathbf{X}^{\mathrm{T}}\mathbf{g}\mathbf{X} = \mathbf{x}\cdot\mathbf{x} - ||\mathbf{x}||^2 = ||\mathbf{x}||^2 - ||\mathbf{x}||^2 = 0, \tag{5}$$

where the dot between two n-dimensional vectors denotes their Euclidean inner product. The cone condition is thus the most natural constraint that we can impose on the dynamical system described in Eq. (2).

Consequently, we have an $(n+1)$-dimensional augmented system:

$$\dot{\mathbf{X}} = \mathbf{A}\mathbf{X} \tag{6}$$

with a constraint of Eq. (3), where

$$\mathbf{A} := \begin{bmatrix} \mathbf{0}_{n\times n} & \frac{\mathbf{f}(\mathbf{x},t)}{||\mathbf{x}||} \\ \frac{\mathbf{f}^T(\mathbf{x},t)}{||\mathbf{x}||} & 0 \end{bmatrix}, \tag{7}$$

satisfying

$$\mathbf{A}^{\mathrm{T}}\mathbf{g} + \mathbf{g}\mathbf{A} = 0 \tag{8}$$

is a Lie algebra $so(n, 1)$ of the proper orthochronous Lorentz group $SO_o(n, 1)$. This fact prompts us to devise the so-called group-preserving schemes, whose discretized maps $\mathbf{G}$ exactly preserve the following properties:

$$\mathbf{G}^{\mathrm{T}}\mathbf{g}\mathbf{G} = \mathbf{g}, \tag{9}$$

$$\det \mathbf{G} = 1, \tag{10}$$

$$\mathbf{G}_0^0 > 0, \tag{11}$$

where $\mathbf{G}_0^0$ is the 00th component of $\mathbf{G}$. Such $\mathbf{G}$ is a proper orthochronous Lorentz group denoted by $SO_o(n, 1)$. The term orthochronous used in the special relativity theory is referred to the preservation of the time orientation. However, it should be understood here as the preservation of the sign $||\mathbf{x}||$.

Remarkably, the original n-dimensional dynamical system of Eq. (1) in E^n can be embedded naturally into an augmented $(n+1)$-dimensional dynamical system of Eq. (6) in M^{n+1}. Although the dimension of the new system is raised by one, it has been shown that the new system has the advantage of devising group-preserving numerical scheme as follows [3]:

$$\mathbf{X}_{\ell+1} = \mathbf{G}(\ell)\mathbf{X}_\ell, \tag{12}$$

where $\mathbf{X}_\ell$ denotes the numerical value of $\mathbf{X}$ at the discrete time t_ℓ, and $\mathbf{G}(\ell) \in SO_o(n, 1)$ is the group value at time t_ℓ.

The group generated from $\mathbf{A} \in SO_o(n, 1)$ is known as a proper orthochronous Lorentz group, of which the Cayley transform

$$\mathrm{Cay}(\tau\mathbf{A}) = (\mathbf{I} - \tau\mathbf{A})^{-1}(\mathbf{I} + \tau\mathbf{A}) \tag{13}$$

is a map from $\mathbf{A}$ to an element of SO_o $(n,1)$ for $\tau \in \mathsf{R}$ and $\tau < ||\mathbf{x}||/||\mathbf{f}||$. Substituting Eq. (7) for $\mathbf{A}(\ell)$, which denotes the values of $\mathbf{A}$ at the discrete time t_ℓ, into the above equation yields

$$\mathrm{Cay}[\tau\mathbf{A}(\ell)] = \begin{bmatrix} \mathbf{I}_n + \frac{2\tau^2\mathbf{f}_\ell\mathbf{f}_\ell^{\mathrm{T}}}{||\mathbf{x}_\ell||^2-\tau^2||\mathbf{f}_\ell||^2} & \frac{2\tau||\mathbf{x}_\ell||\mathbf{f}_\ell}{||\mathbf{x}_\ell||^2-\tau^2||\mathbf{f}_\ell||^2} \\ \frac{2\tau||\mathbf{x}_\ell||\mathbf{f}_\ell^{\mathrm{T}}}{||\mathbf{x}_\ell||^2-\tau^2||\mathbf{f}_\ell||^2} & \frac{||\mathbf{x}_\ell||^2+\tau^2||\mathbf{f}_\ell||^2}{||\mathbf{x}_\ell||^2-\tau^2||\mathbf{f}_\ell||^2} \end{bmatrix}. \tag{14}$$

Inserting the above $\mathrm{Cay}[\tau\mathbf{A}(\ell)]$ for $\mathbf{G}(\ell)$ into Eq. (12) and ranking its first row, we obtain

$$\mathbf{x}_{\ell+1} = \mathbf{x}_\ell + hw(\ell)\mathbf{f}_\ell, \tag{15}$$

where

$$w(\ell) := \frac{||\mathbf{x}_\ell||^2 + \tau\mathbf{f}_\ell\cdot\mathbf{x}_\ell}{||\mathbf{x}_\ell||^2 - \tau^2||\mathbf{f}_\ell||^2}, \tag{16}$$

is called a weighting factor. In the above, $\mathbf{x}_\ell$ denotes the numerical value of $\mathbf{x}$ at the discrete time t_ℓ, τ is one half of the time increment, i.e., $\tau := h/2$, and more precisely, $\mathbf{f}_\ell$ is $\mathbf{f}(\mathbf{x}_\ell, t_\ell)$.

In order to meet the property of Eq. (11), we require the step-size of the scheme of Eq. (15) being constrained by $h<2||\mathbf{x}_\ell||/||\mathbf{f}_\ell||$. Under this condition, we have

$$h<\frac{2||\mathbf{x}_\ell||}{||\mathbf{f}_\ell||} \Leftrightarrow G_0^0>0 \Rightarrow w(\ell)>0. \tag{17}$$

3. A new time step-size adaptive numerical scheme

It deserves to note that the scheme of Eq. (15) is very similar to the Euler scheme,

$$\mathbf{x}_{\ell+1} = \mathbf{x}_\ell + \Delta t \mathbf{f}_\ell, \tag{18}$$

where Δt is a fixed time step-size. This motivates us to derive a new time step-size adaptive numerical scheme

$$\mathbf{x}_{\ell+1} = \mathbf{x}_\ell + h\mathbf{f}_\ell \tag{19}$$

where h is varying step-by-step and is solved from the following equation:

$$\frac{||\mathbf{x}_\ell||^2 + \tau \mathbf{f}_\ell \cdot \mathbf{x}_\ell}{||\mathbf{x}_\ell||^2 - \tau^2||\mathbf{f}_\ell||^2} h = \Delta t, \tag{20}$$

which is obtained by letting the coefficient in Eq. (15) equal to Δt.

Upon noting that $\tau = h/2$, from Eq. (20) we obtain

$$[\Delta t||\mathbf{f}_\ell||^2 + 2\mathbf{f}_\ell \cdot \mathbf{x}_\ell]h^2 + 4||\mathbf{x}_\ell||^2 h - 4\Delta t||\mathbf{x}_\ell||^2 = 0. \tag{21}$$

The discriminant of Eq. (21) is non-negative as shown in the following:

$$\begin{aligned} &16||\mathbf{x}_\ell||^4 + 16\Delta t||\mathbf{x}_\ell||^2\left[\Delta t||\mathbf{f}_\ell||^2 + 2\mathbf{f}_\ell \cdot \mathbf{x}_\ell\right] \\ &= 16||\mathbf{x}_\ell||^2||\mathbf{x}_\ell + \Delta t\mathbf{f}_\ell||^2 \geqslant 0. \end{aligned} \tag{22}$$

Depending on the sign of the coefficient before h^2 in Eq. (21), there have three possible conditions:

$$\left(\Delta t\|\mathbf{f}_\ell\|^2 + 2\mathbf{f}_\ell \cdot \mathbf{x}_\ell\right) > 0, \text{ one positive root and one negative root,} \tag{23}$$

$$\left(\Delta t||\mathbf{f}_\ell||^2 + 2\mathbf{f}_\ell \cdot \mathbf{x}_\ell\right) = 0, \text{ double root with } h = \Delta t, \tag{24}$$

$$\left(\Delta t||\mathbf{f}_\ell||^2 + 2\mathbf{f}_\ell \cdot \mathbf{x}_\ell\right) < 0, \text{ two positive roots.} \tag{25}$$

In summary, we only consider the positive root, which is given by

$$h(\ell) = \frac{2||\mathbf{x}_\ell||(||\mathbf{x}_\ell + \Delta t\mathbf{f}_\ell|| - ||\mathbf{x}_\ell||)}{\Delta t||\mathbf{f}_\ell||^2 + 2\mathbf{f}_\ell \cdot \mathbf{x}_\ell}. \tag{26}$$

In the above, we have seen that only in the limiting case with that in Eq. (24), $h = \Delta t$; therefore, it is very interesting for us to know that when $h>\Delta t$ and when $h<\Delta t$?

In the coefficient before h^2 in Eq. (21), the sign is dominated by the quantity, $\mathbf{f} \cdot \mathbf{x}$, because $\Delta t||\mathbf{f}||^2$ is a small number. Therefore, we can use $\mathbf{f} \cdot \mathbf{x}$ as a criterion to choose h as shown in Fig. 1. We give a geometric description as follows. When the quantity $\mathbf{f} \cdot \mathbf{x}>0$, the vector $\mathbf{f}$ is moving in the direction outwards, and the norm $||\mathbf{x}||$ will increase relatively. In the contrast, when $\mathbf{f} \cdot \mathbf{x}<0$, the vector $\mathbf{f}$ is moving in the direction inwards, and the norm $||\mathbf{x}||$ will decrease relatively.

In the Euler scheme, no matter what condition is, its step-size is always Δt, which however as mentioned in Section 1, would likely lead to numerical instability. In our new method, $\mathbf{f} \cdot \mathbf{x}$ is adopted as a criterion to adapt h to avoid numerical instability; however, h and Δt must satisfy Eq. (21) simultaneously. In this regard, the

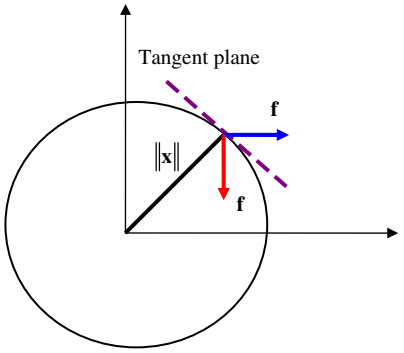

Fig. 1. The changing relation of the vector-value function **f** and the Euclidean norm||**x**|| in a domain.

new method has two kinds of conditions as follows:

$$h<\Delta t, \text{ when } \mathbf{f}\cdot\mathbf{x}>0,$$
$$h>\Delta t, \text{ when } \mathbf{f}\cdot\mathbf{x}<0.$$

The above two statements are rather significant in that when the vector field tends to increase the magnitude ||**x**||, the new method will adopt a smaller time step-size to avoid numerical instability, and conversely, when the vector field tends to decrease the magnitude ||**x**||, the new method will adopt a larger time step-size to save computation time.

Substituting Eq. (26) for $h(\ell)$ into Eq. (19), we obtain a time step-size adaptive numerical scheme as follows:

$$\mathbf{x}_{\ell+1}=\mathbf{x}_\ell+\frac{2||\mathbf{x}_\ell||(||\mathbf{x}_\ell+\Delta t\mathbf{f}_\ell||-||\mathbf{x}_\ell||)}{\Delta t||\mathbf{f}_\ell||^2+2\mathbf{f}_\ell\cdot\mathbf{x}_\ell}\mathbf{f}_l. \tag{27}$$

Specially, we call the ratio $\eta(\ell):=h(\ell)/\Delta t$ an adaptive factor of the scheme in Eq. (19). In numerical implementation we do not need to adjust the step size, because our $h(\ell)$ is adapted automatically according to the values of $\mathbf{x}_\ell$ and $\mathbf{f}_\ell$ at the previous step.

4. Numerical examples

Example 1 (*Duffing equation*). To test the capability of the numerical scheme developed in Section 3, let us consider the following Duffing equation with forcing term:

$$\ddot{x}+\gamma\dot{x}+\alpha x+\beta x^3=f_0\cos\omega t, \tag{28}$$

which describes the motion of a nonlinear oscillator in the presence of a nonlinear restoring force equal to $\alpha x+\beta x^3$, a damping γ and a periodic driving term with amplitude f_0. Some of the earliest observations of chaotic attractors were made on this equation, which exhibits a rich variety of chaotic phenomena in various parameters regimes. We apply the GPS and the time step-size adaptive scheme shown in Section 3 to solve the Duffing equation, where the parameters $\alpha=-1$, $\beta=1$, $\gamma=1$, and $\omega=1.2$ with the amplitudes of the imposed forces f_0 given as 0.2, 0.27, 0.2861, 0.2867 and 0.32, respectively. Numerical results of the time step-size adaptive scheme are shown in Fig. 2, where the trajectories of the Duffing equation are plotted in Figs. 2(a),(d),(g),(j) and (m) with respect to one-period, two-period, four-period, eight-period and chaos response, respectively. It should be noted that the transient part of the trajectories which starting from the initial point $x_1=2$ and $x_2=0$ are not plotted in these figures. At the same time we plot the time histories and power spectrum of the adaptive factor η in Figs. 2(b),(e),(h),(k) and (n) and Figs. 2(c),(f),(i),(l) and (o), respectively. Similarly, numerical results of the GPS are shown in Fig. 3 including the trajectories of the Duffing equation shown in Figs. 3(a),(d),(g),(j) and (m), and the time histories and power spectrum of the weighting factor w shown in Figs. 3(b),(e),(h),(k) and (n) and Figs. 3(c),(f),(i),(l) and (o), respectively. It should

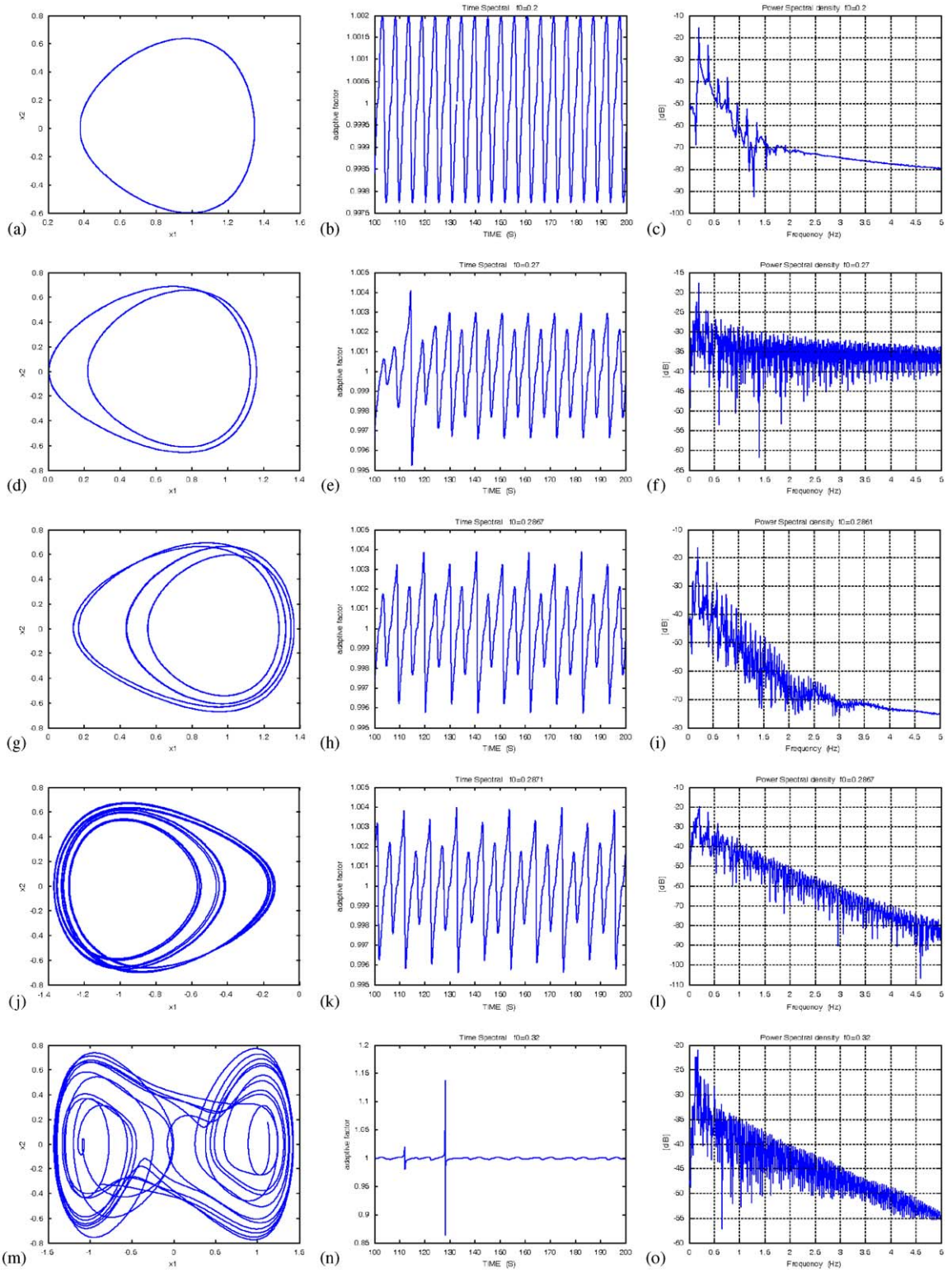

Fig. 2. Results obtained for Duffing equation using time step-size adaptive numerical scheme in Section 3. The sequences of period-doubling to chaos are shown in the left column; while time histories and power spectrum of the adaptive factor η are shown in the middle and right column, respectively.

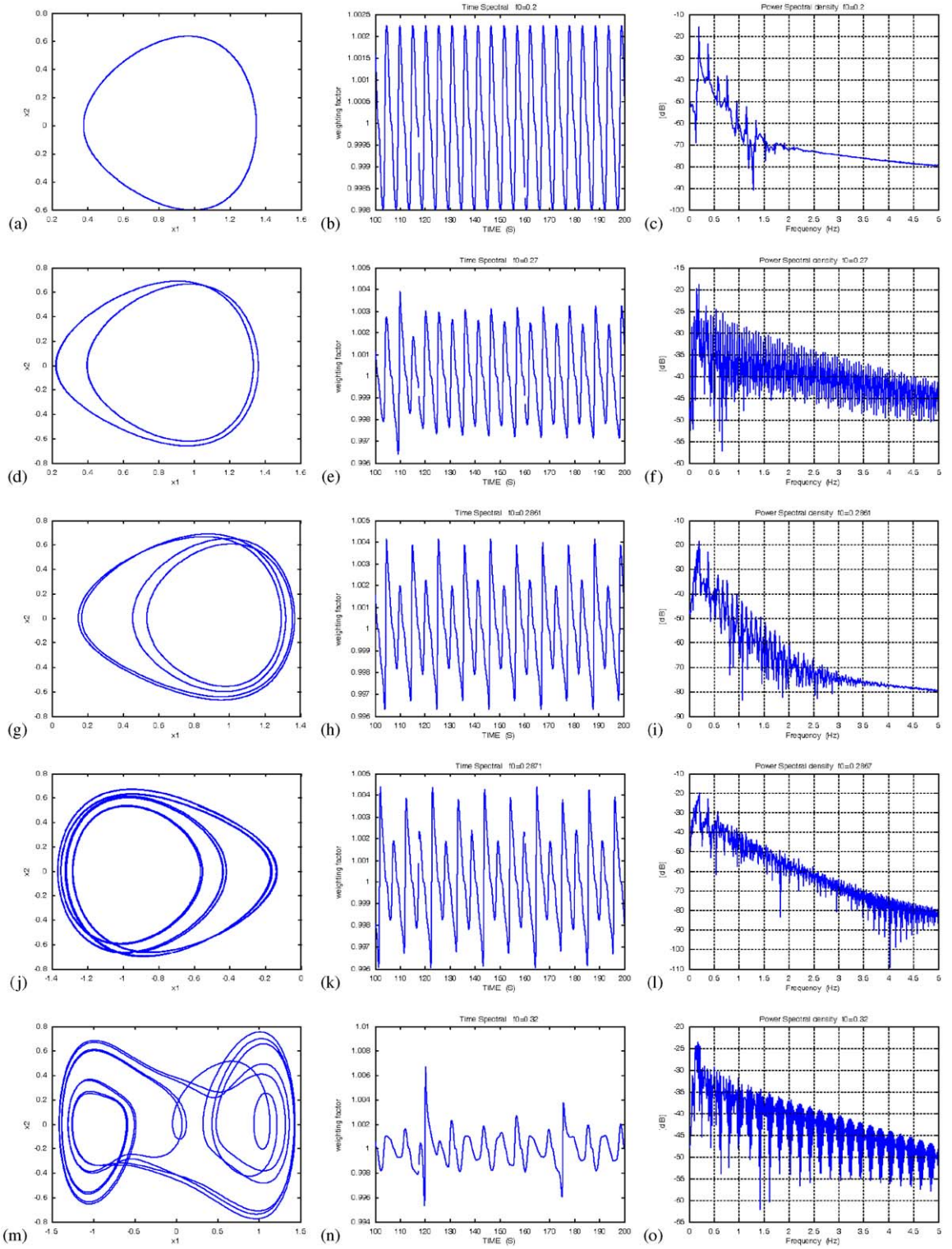

Fig. 3. Results obtained for Duffing equation using the GPS in Section 2. The sequences of period-doubling to chaos are shown in the left column; while time histories and power spectrum of the weighting factor w are shown in the middle and right column, respectively.

be noted that although the proposed time step-size adaptive scheme has no dominant effect on computing time as compared with the GPS, yet the proposed adaptive scheme can show more detailed dynamic behaviors in the chaotic state without loss of its computational accuracy as shown in Figs. 2(m) and 3(m).

Example 2 (*Lorenz system [10]*). A seminal example of chaotic flow that arises from the hydrodynamic equations for describing the Rayleigh–Bénard convections is the Lorenz system

$$\begin{aligned} \dot{x} &= -\sigma x + \sigma y, \\ \dot{y} &= Rx - y - xz, \\ \dot{z} &= xy - Bz. \end{aligned} \tag{29}$$

The numbers σ, B and R are the system's physical parameters, which Lorenz fixed them at $\sigma = 10$, $B = 8/3$ and $R = 26$. Again two types of numerical schemes including the GPS and the time step-size adaptive one are adopted to solve the Lorenz system. Numerical results of the time step-size adaptive scheme are shown in Fig. 4, in which the trajectories of Lorenz system are plotted in Figs. 4(a) and (b). The transient part of the

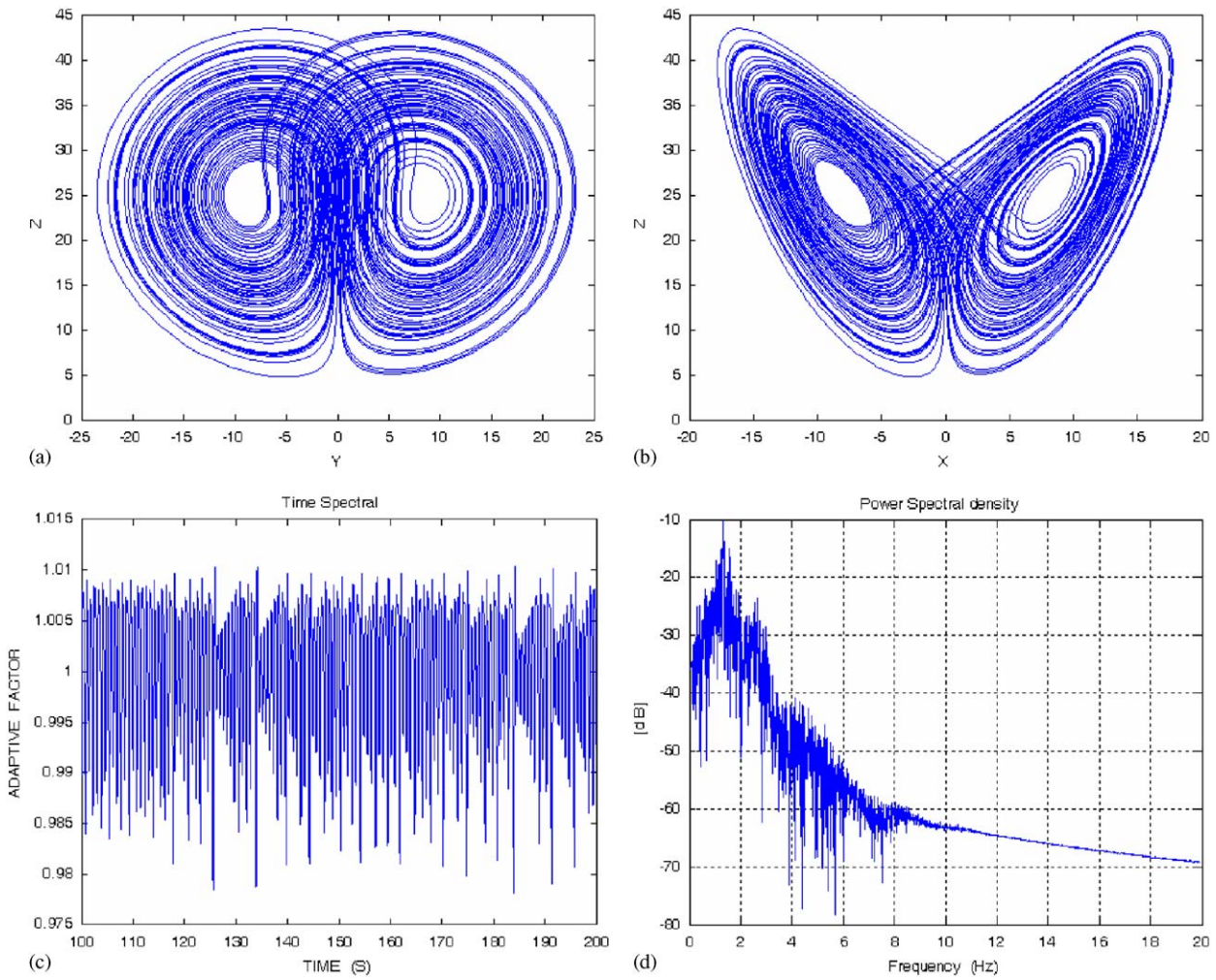

Fig. 4. Results obtained for the Lorenz system using the time step-size adaptive numerical scheme. Trajectories of the Rössler system are shown in (a) and (b); while time histories and power spectrum of the adaptive factor η are shown in (c) and (d).

trajectories which starting from the initial point $x = 1.0$, $y = 1.0$ and $z = 0$ are not plotted in the figures. However, we plot the time histories and power spectrum of the adaptive factor η in Figs. 4(c) and (d), respectively. Similarly, numerical results of the GPS are shown in Fig. 5, in which the trajectories of Lorenz system are shown in Figs. 5(a) and (b), and the time histories and power spectrum of the weighting factor w are shown in Figs. 5(c) and (d), respectively.

Example 3 (*Rössler system*). In 1976, Rossler [11] found a particularly simple system, which is probably the most elementary geometric construction of chaos in continuous systems, and be designed solely with the purpose of creating a model for a strange attractor using only the simplest chaos generating mechanism, stretch-and-fold. The Rössler system we consider is the following equations system:

$$\begin{aligned} \dot{x} &= -(y + z), \\ \dot{y} &= x + ay, \\ \dot{z} &= b + xz - cz, \end{aligned} \tag{30}$$

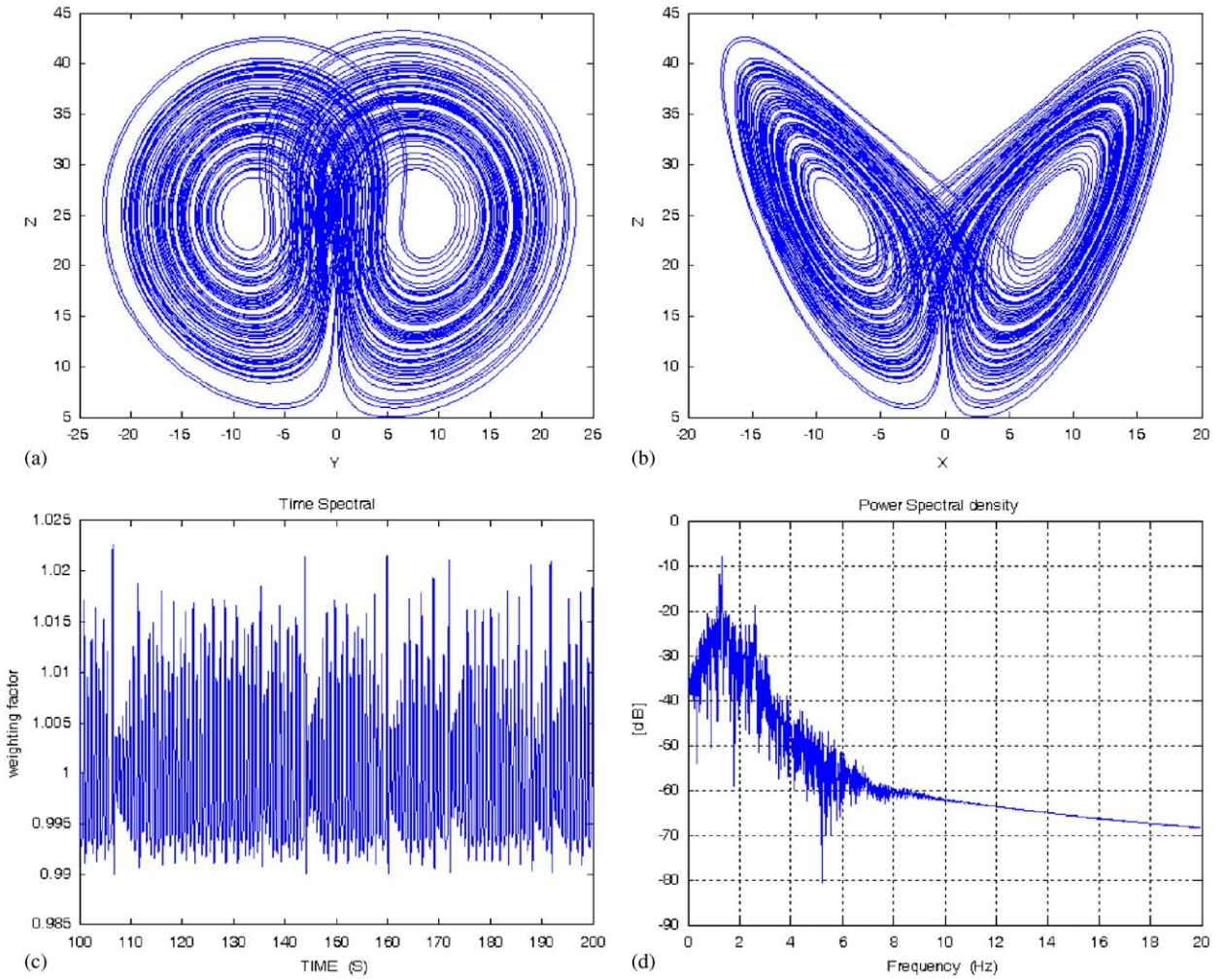

Fig. 5. Results obtained for the Lorenz system using the GPS numerical scheme. Trajectories of the Rössler system are shown in (a) and (b); while time histories and power spectrum of the weighting factor w are shown in (c) and (d).

where a, b and c are adjustable constants. Again two types of numerical schemes including the GPS and the time step-size adaptive one are adopted to solve the Rössler system. The parameters of the Rössler system are fixed at $a = b = 1/5$, and $c = 5.7$. Numerical results of the time step-size adaptive scheme are shown in Fig. 6, in which the trajectories of Rössler system are shown in Figs. 6(a) and (b). The transient part of the trajectories which starting from the initial point $x = -1.0$, $y = 0$ and $z = 0$ is not plotted in the figures; however, we plot the time histories and power spectrum of the adaptive factor η in Figs. 6(c) and (d), respectively. Similarly, numerical results of the GPS are shown in Fig. 7, in which the trajectories of the Rössler system are shown in Figs. 7(a) and (b), and the time histories and power spectrum of the weighting factor w are shown in Figs. 7(c) and (d), respectively.

Example 4. In this example [12], we will solve the response problem of the nonlinear periodic system:

$$\begin{aligned} \dot{x}_1 &= x_2, \\ \dot{x}_2 &= -2.25x_1 - (x_1 - 1.5 \sin t)^3 + 2 \sin t, \\ x_1(0) &= 0.0, \quad x_2(0) = 1.59929. \end{aligned} \tag{31}$$

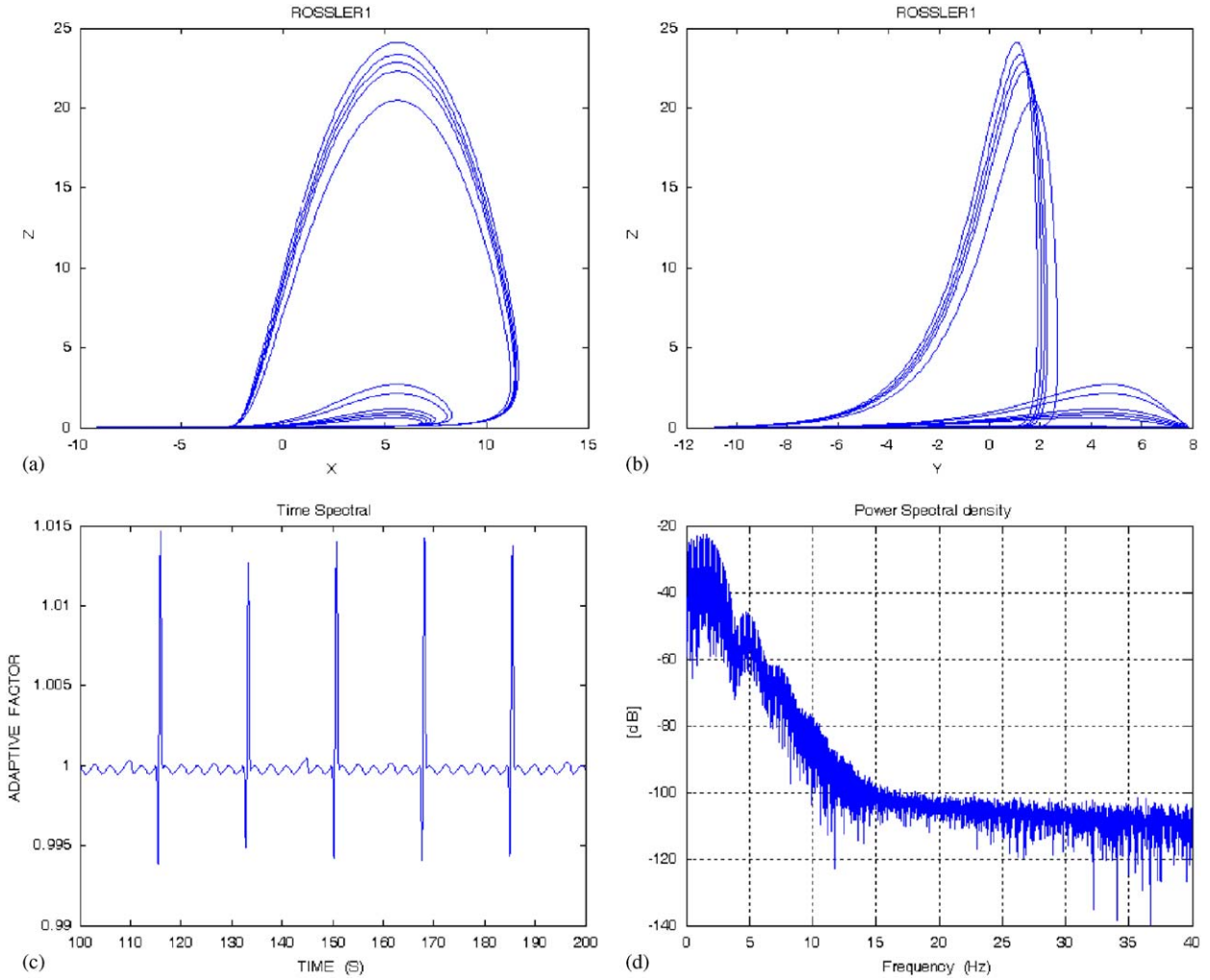

Fig. 6. Results obtained for the Rössler system using the time stepsize adaptive numerical scheme. Trajectories of the Rössler system are shown in (a) and (b); while time histories and power spectrum of the adaptive factor η are shown in (c) and (d).

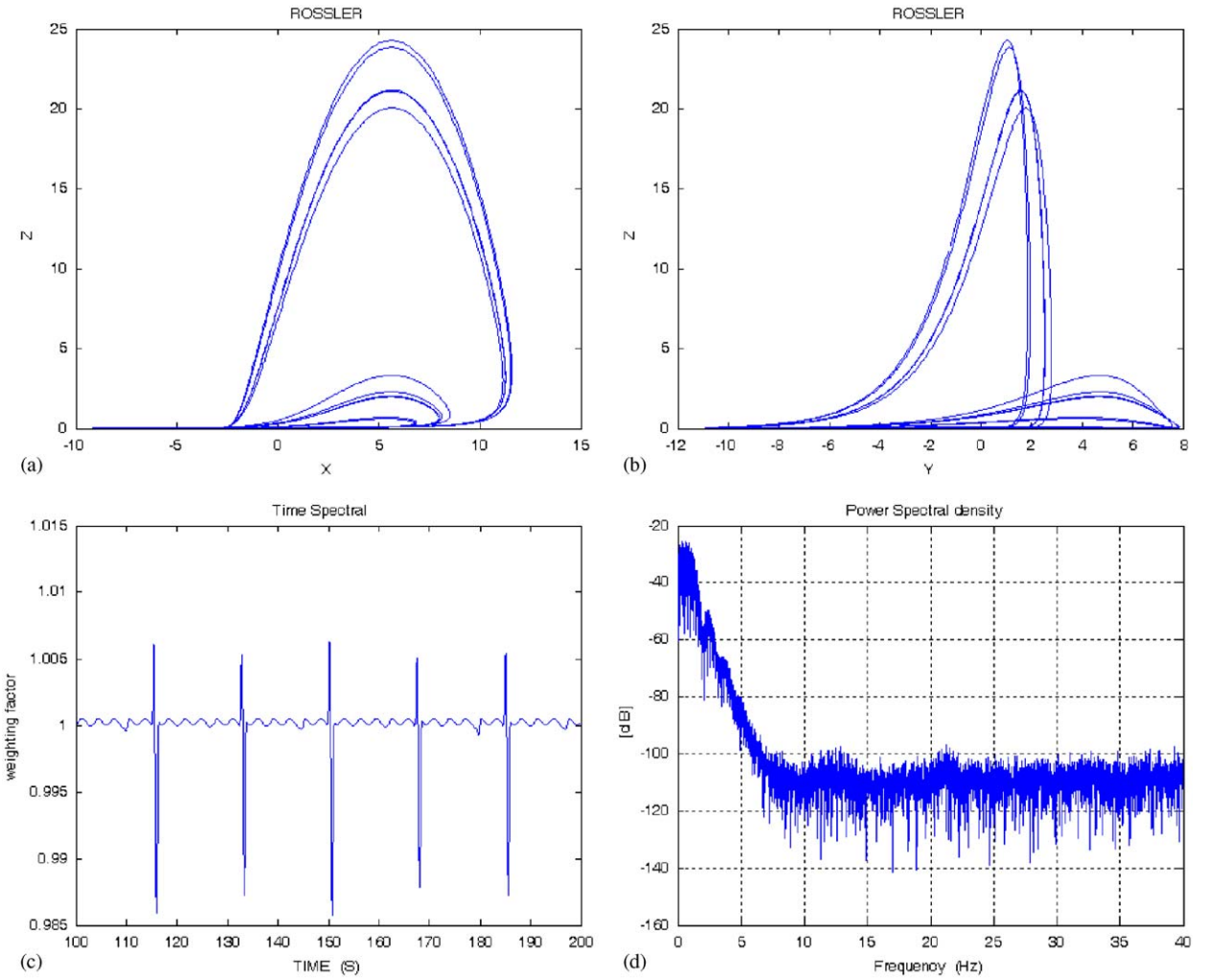

Fig. 7. Results obtained for the Rössler system using the GPS numerical scheme. Trajectories of the Rössler system are shown in (a) and (b); while time histories and power spectrum of the weighting factor w are shown in (c) and (d).

Their exact solutions are

$$x_1(t) = 1.59941 \sin t - 0.00004 \sin 3t,$$
$$x_2(t) = 1.59941 \cos t - 0.00012 \cos 3t. \tag{32}$$

The GPS and the time step-size adaptive scheme are adopted to solve the nonlinear periodic system. Comparisons of the numerical results are shown in Fig. 8, in which the errors of numerical solutions with respect to the exact solution for x_1 and x_2 are shown in Figs. 8(a) and (b), respectively, and the trajectories of nonlinear periodic system are plotted in Fig. 8(c). Since the exact solution is available in this example, it is shown that the proposed time step-size adaptive scheme has the same accuracy as the GPS and both schemes are reliably demonstrated.

Example 5. Here, we consider the following initial-value problem for the ordinary differential equations [12]:

$$\ddot{x} = -(\dot{x})^2 - x + \ln t, \quad x(1) = 0, \quad \dot{x}(1) = 1. \tag{33}$$

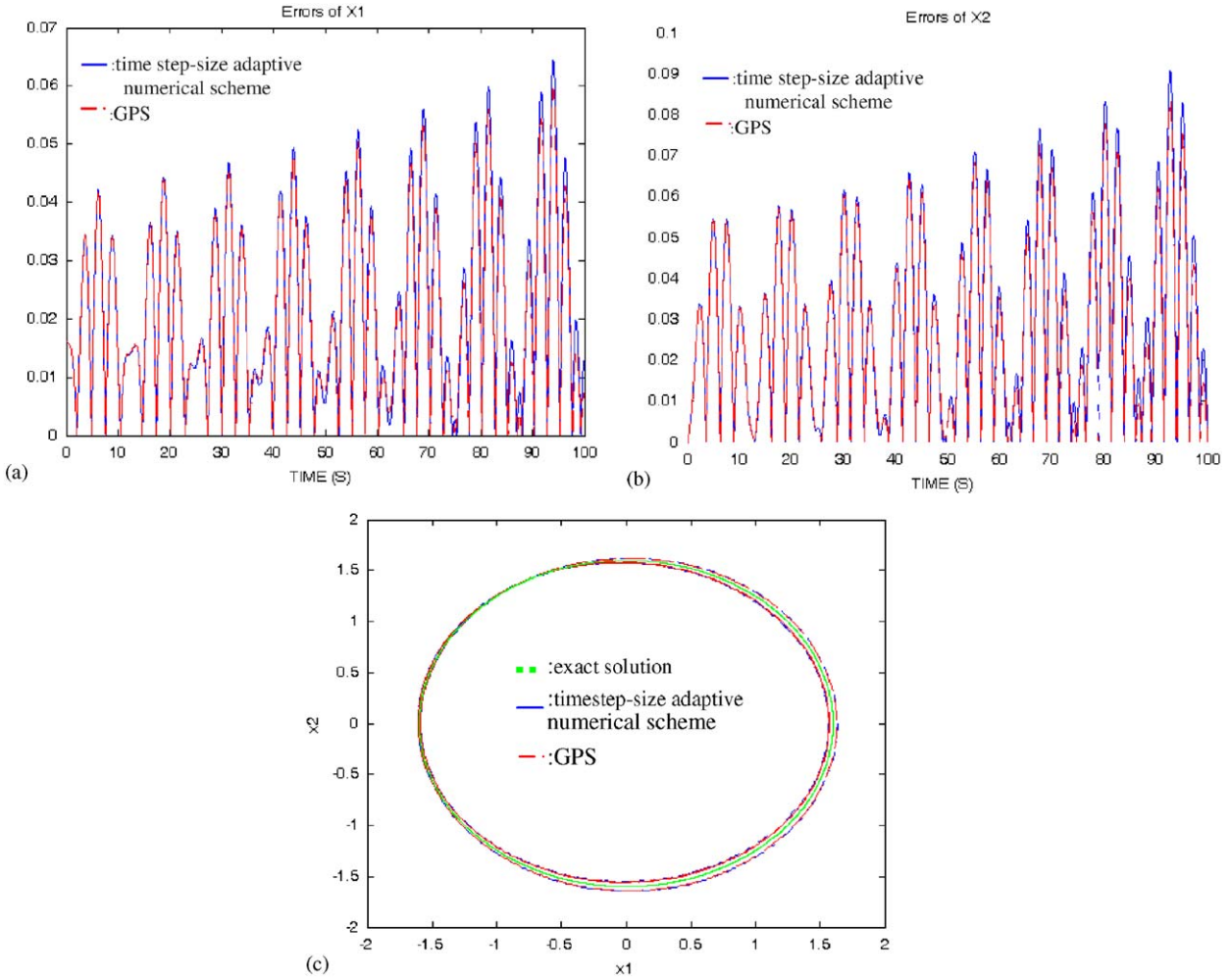

Fig. 8. Results obtained for the nonlinear periodic system using the GPS and the time step-size adaptive numerical scheme. Errors of numerical solutions with respect to the exact solution are shown in (a) and (b), and trajectories of nonlinear periodic system are plotted in (c).

Its exact solution is

$$x = \ln t. \tag{34}$$

The above second-order ordinary differential equation can be transformed into the following first-order differential equation:

$$\begin{aligned} \dot{x}_1 &= x_2, & x_1(1) &= 0, \\ \dot{x}_2 &= -x_1 - x_2^2 - x + \ln t, & x_2(1) &= 1. \end{aligned} \tag{35}$$

Then, we use the GPS and the time step-size adaptive scheme, respectively, to solve the above equations. Fig. 9(a) shows the errors of numerical solutions with respect to the exact solution for the GPS and the time step-size adaptive schemes, respectively. Fig. 9(b) shows time trajectories of the two schemes with the exact solution. Sound matching results in these two figures again validate the accuracy of the proposed scheme.

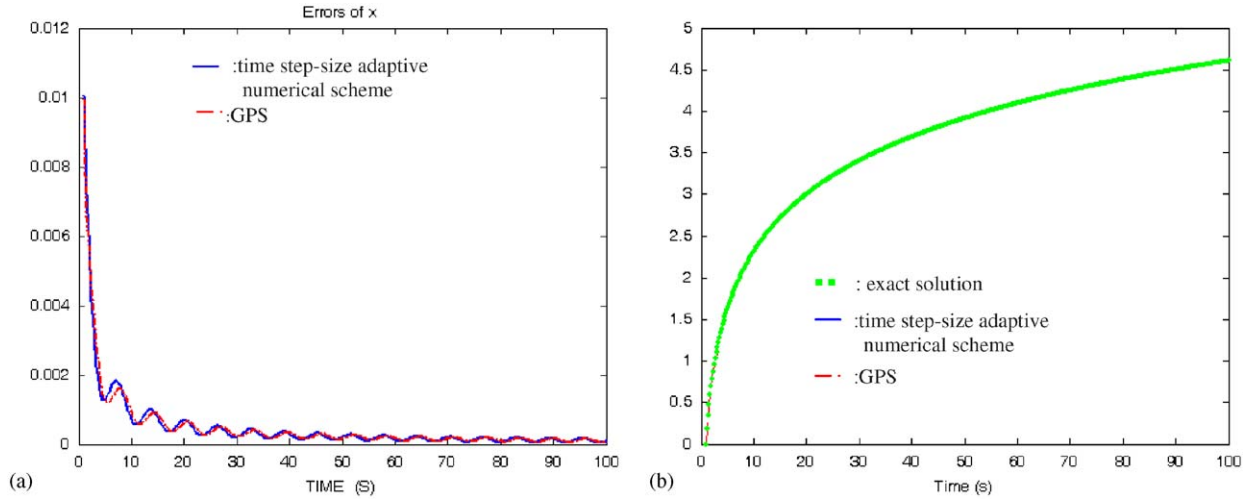

Fig. 9. Results obtained for the initial-value problem of ordinary differential equations using the GPS and the time step-size adaptive numerical scheme. Errors of numerical solutions with the exact solution for the GPS and the time step-size are shown in (a) and time trajectories of the two schemes with the exact solution are shown in (b).

5. Concluding remarks

In this paper, we have proposed a time step-size automatically adaptive numerical scheme to calculate the responses of nonlinear dynamical systems. Our method is drastically different from the conventional variable step-size schemes, the step-sizes of which are usually controlled by meeting the specified accuracy, and their numerical implementations are rather complicated. Numerical examples show that the time histories of the adaptive factor can reflect the information of the chaotical motion. When the system is in the non-chaotic state, the adaptive factor has regular time history; however, when the system is in the chaotic state, the adaptive factor has irregular time history. Besides, the proposed adaptive scheme can show more detailed dynamic behaviors without loss of the accuracy in the chaotic state of the nonlinear dynamic system as compared with the GPS.

References

[1] B. Chen, F. Solis, Discretizations of nonlinear differential equations using explicit finite order methods, *Journal of Computational and Applied Mathematics* 90 (1998) 171–183.
[2] R.E. Mickens, *Nonstandard Finite Difference Model of Differential Equations*, World Scientific, Singapore, 1994.
[3] C.S. Liu, Cone of non-linear dynamical system and group preserving schemes, *International Journal of Non-Linear Mechanics* 36 (2001) 1047–1068.
[4] S. Boccaletti, C. Grebogi, Y.C. Lai, H. Mancini, D. Maza, The control of chaos: theory and applications, *Physics Reports* 329 (2000) 103–197.
[5] K.I.R. Moorthy, A. Kakodkar, The significance of higher modes for evolution on chaos in structural mechanics systems, *Journal of Sound and Vibration* 198 (1996) 267–277.
[6] A.A. Al-Qaisia, M.N. Hamdan, Bifurcations of approximate harmonic balance solutions and transition to chaos in an oscillator with inertial and elastic symmetric nonlinearities, *Journal of Sound and Vibration* 244 (2001) 453–479.
[7] A.A. Al-Qaisia, M.N. Hamdan, Bifurcations and chaos of an Immersed cantilever beam in a fluid and carrying an intermediate mass, *Journal of Sound and Vibration* 253 (2002) 859–888.
[8] Z.M. Ge, T.C. Yu, Y.S. Chen, Chaos synchronization of a horizontal platform system, *Journal of Sound and Vibration* 268 (2003) 731–749.
[9] J.J. Lou, S.J. Zhu, L. He, X. Yu, Application of chaos method to line spectra reduction, *Journal of Sound and Vibration* 286 (2005) 645–652.
[10] E.N. Lorenz, Deterministic nonperiodic flow, *Journal the Atmospheric Science* 20 (1963) 130–141.
[11] O.E. Rössler, An equation for continuous chaos, *Physics Letter A* 35 (1976) 397–398.
[12] S.Y. Zhang, Z.C. Deng, Group preserving schemes for nonlinear dynamic system based on RKMK methods, *Applied Mathematics and Computation* 175 (2006) 497–507.